



Effect of temperature on properties of cadmium sulfide nanostructures synthesized by solvothermal method

Jaya Khatter¹ · R. P. Chauhan¹

Received: 12 September 2019 / Accepted: 21 December 2019 / Published online: 4 January 2020
© Springer Science+Business Media, LLC, part of Springer Nature 2020

Abstract

Large surface area to volume ratio of the nanostructured materials is familiar to play an important role in novel catalytic, sensing and optoelectronics application. In current research work, CdS nanostructures are synthesized by solvothermal process. This synthesis is carried out at different temperatures of 140 °C, 160 °C, 180 °C and 200 °C. The structural, morphological, optical, elemental and electrical properties of cadmium sulfide nanostructures are investigated using X-Ray Diffractometry (XRD), Field Emission Scanning Electron Microscope (FESEM), UV–Visible spectroscopy, photoluminescence spectrometry (PL), FTIR and two probe set up assisted with Keithley source meter. XRD pattern confirmed the formation of hexagonal wurtzite structure for all the solvothermal temperatures. FESEM analysis depicted the formation of cadmium sulfide nanorods in any possible orientation with high density. EDS is also performed to confirm the elemental composition of CdS nanostructures. The UV–Vis spectroscopy revealed that optical band gap increased at low solvothermal temperature indicating the confinement effects in CdS nanostructures. These cadmium sulfide nanostructures may have the potential application in hydrogen production, optoelectronics devices and gas sensing.

1 Introduction

Dimension plays a crucial role in ruling the material properties. Dimensionality is a significant aspect that distinguishes the nanostructures from their bulk counterparts. One dimensional nanostructures i.e., nanorods, nanotubes, nanowires and nanoribbons are smallest system that leads us to explore the dependence of structural, optical and electrical properties on confinement and dimensionality. Over the last two decades, advanced growth approaches have been developed for the synthesis of nanosized semiconductor material with preferable morphology in a controlled manner. Controlling the size of semiconducting micro/nanocrystals is a critical issue to explore the novel properties of materials in nanotechnology. Semiconducting nanostructures of II–VI group are key elements for recent advanced technologies in the field of optoelectronics, toxic gas sensing, radiation detection, magnetic and photonic devices, and nanoelectronics

and in light emission applications. Group II–VI compound semiconductors composed of a metal from group 12 (formerly called IIB) and other element from group 16 (formerly called VI). These compound semiconductors crystallize in two polymorphs i.e., hexagonal wurtzite and zinc blende. Wide range of direct band gaps is the major motivation to study II–VI semiconductors. The wide band gap covers the infrared to ultraviolet range in electromagnetic spectrum that could be the basis for variety of efficient photonic, optoelectronic and light emission applications. The II–VI semiconducting materials are very interesting from the technological point of view due to their direct band gap, high optical absorption and emission coefficients.

CdS is one of the most investigated II–VI compound semiconductors that exhibit intrinsic n-type of conductivity. Cadmium sulfide has two types of polytypes; hexagonal wurtzite and zinc blende. Studies showed that as the size of CdS nanoparticles decreases, the crystal structure of CdS changes from hexagonal phase to zinc blende [1]. Cadmium sulfide has direct band gap of 2.42 eV which presents the significant field for potential applications in non-linear optics. Cadmium sulfide has unique optical, structural and electrical properties at room temperature. The nanostructures of cadmium sulfide manifest revised physical, chemical and structural properties from the bulk. Cadmium sulfide is

✉ R. P. Chauhan
chauhanrpc@gmail.com

Jaya Khatter
jaya_6180019@nitkkr.ac.in

¹ Department of Physics, National Institute of Technology, Kurukshetra 136119, India

widely used as window layer in solar cell applications due to its wide band gap, high optical transmittance and good electrical properties [2, 3]. Solar energy can easily excite CdS to produce electron hole pair that can be utilized in photo catalytic activity. In recent years, cadmium sulfide nanostructures have received extensive attention as photo catalyst for hydrogen production in the photo electrochemical cell, in degradation of pollutants and in reduction of CO₂. Cadmium sulfide nanoparticles have been widely used for photo degradation of inorganic or organic pollutants in air and water. In terms of solar-fuel generation and environmental purification, CdS and their composite nanostructures exhibits the excellent photo catalytic properties. The aspect ratio and morphology of nanostructured materials appreciably affect their catalytic property since they perturb the available surface area, light absorption and the charge carrier dynamics [4, 5].

Semiconducting nanowire-based detection approaches provide a promising route for ultra-sensitive electric detection. Vanalakar et al. [6] reported synthesis of the cadmium sulfide nanowire mesh for NO₂ sensing. The inter-wire space distance, as well as densities of the nanowires, was observed to play a crucial role in the gas adsorption–desorption reaction, enabling an improvement in the gas sensing properties. This CdS NW mesh showed 50-fold better sensitivity towards NO₂ sensing than earlier reports. CdS nanostructures are also investigated for visible and ultraviolet light detection. Highly efficient and sensitive broad-band UV/visible/near infrared self-powered photo detectors have been fabricated based on n-type CdS and p-type P3HT involve a p–n junction that contributes to the self-powered photo detection [7, 8]. One dimensional II–VI nanostructures have raised significant attention in electronic and optoelectronic devices owing to their high sensitivity and quantum efficiency. One dimensional geometry is profitable for quick and long distance electron transport. II–VI nanostructures with one dimensionality have been proposed for advanced novel applications due to their specific geometry and distinct properties. Enormous attempts have been made to synthesize one dimensional nanostructure in recent years. Proper understanding of synthesis of the nano-material and designing of device structure is still an important challenge to explore the industrial applications. And higher flexibility of nanostructure growth is also an important challenge because it is very complicated to synthesize desired nanostructures. Therefore, it becomes important to make the appreciable attempts to synthesize the CdS nanostructures of different morphologies. Several techniques such as chemical vapor deposition [9], hydrothermal [10], laser ablation [11] and electro deposition [12] methods have been used to synthesize the one dimensional nanostructures. Among these techniques, the hydrothermal or solvothermal (solvent is used instead of aqueous medium) method is an attractive method for the preparation of 1-D nanostructures with the advantage

of simplicity and easy control of morphology by changing the temperature, precursor concentration and reaction time.

Various surfactant or capping agents are utilized in the growth of nanostructures. Polyvinylpyrrolidone (PVP) is used as stabilizer with C–N, C=O and CH₂ functional group. PVP is widely used in synthesis of nanoparticles as a surface stabilizing agent, growth modifier and reducing agent depending on the reaction conditions. PVP is non-ionic, bulky and biocompatible polymer that extensively used in nanoparticles synthesis. A PVP molecule incorporates pyrrolidone part (hydrophilic) and alkyl group (hydrophobic). The PVP serves either in controlling the growth of nanostructures by forming layer around the compound or in preventing the agglomeration of nanoparticles by steric hindrance effect [13]. Generally, C=O of PVP made complexes with Cd²⁺ ions and selectively adsorb on the surface of CdS. Adsorption results into suppressing of the nanoparticles growth and resulting into extremely small particles. The usage of PVP also counters the aggregation of nanoparticles due to repulsive forces among the hydrophobic carbon [14]. Qingqing et al. observed that cadmium sulfide nanoparticles could be tuned into elongated nanorods by using PVP as surfactant. The amount of PVP plays an essential role in controlling the size, shape and optical properties of CdS. The formation of elongated nanorods favored at high PVP concentration but excess amount of PVP restricted the nanoparticles growth in various directions [15]. Hui Qi et al. also synthesized the one dimensional CuS microstructures by microwave hydrothermal method by using PVP as stabilizer. This study also demonstrated the usage of high PVP concentration resulting into the formation of elongated one dimensional nanostructure [16]. Xia et al. [17] synthesized the polycrystalline walnut like CdS nanostructures by solvothermal method. The factors i.e., PVP amount, reaction time and temperature are found to be productive in tailoring the size, shape, morphology of nanostructures. Moreover, these factors also affect the optical properties.

In the present work, PVP capped CdS nanostructures are synthesized using ethylenediamine as solvent agent. Several studies have revealed the effect of PVP and ethylenediamine in synthesis of nanostructures. To the best of author knowledge, no studies have been made for incorporated study of PVP surfactant with ethylenediamine in synthesis of cadmium sulfide nanostructures. In this study, an attempt has been made to study the effect of reaction temperature on crystallinity, morphology, electrical and optical properties of the PVP capped CdS nanostructures.

2 Experimental procedure

For the synthesis of CdS nanostructures, cadmium acetate dihydrate [Cd (CH₃COO)₂·2H₂O] and thiourea [NH₂CSNH₂] purchased from Sigma Aldrich are used. The

other chemicals such as polyvinylpyrrolidone (PVP) and ethylenediamine [$C_2H_8N_2$] are of analytical grade and purchased from Loba Chemie. All chemicals are used without any further purification.

In this synthesis, 0.12 M cadmium acetate dihydrate and 0.34 M thiourea are dispersed in 80 ml solution (Ethylenediamine and DI water in ratio 3:1) and PVP is added into the precursor solution and stirred for 1 h to get a transparent solution. After that, this solution is transferred into 100 ml Teflon lined stainless steel autoclave at different growth temperatures of 140 °C, 160 °C, 180 °C and 200 °C for 20 h each. These samples are marked as CdS-140, CdS-160, CdS-180 and CdS-200, respectively. Then, the autoclave is allowed to cool down to room temperature. Then the precipitates are filtered off and washed with DI water and ethyl alcohol. The product is placed in the oven to dry out for 12 h at 80 °C. A schematic diagram demonstrating the solvothermal synthesis of CdS nanostructures is shown in Fig. 1.

3 Characterizations

The crystallography of as-synthesized cadmium sulfide nanostructures is examined with the help of Rigaku Mini-Flex II X-Ray diffractometer using a Ni-filtered Cu K_{α} radiation ($\lambda = 1.54 \text{ \AA}$) with a scanning rate of $2^\circ/\text{min}$. in 2θ range of 20° to 80° . The morphology of CdS nanostructures is analyzed by Field Emission Scanning Electron Microscopy (FESEM) for which sample is coated with gold palladium alloy to make a conducting layer on it. Energy Dispersive X-Ray spectroscopy is also performed to probe the elemental composition of CdS nanostructures. The optical properties of cadmium sulfide samples are studied with UV–Vis spectrophotometer while photoluminescence spectra are taken at room temperature on spectrofluorophotometer. A two probe

setup along with Keithley 2400 source meter is utilized to study the electrical properties of CdS nanostructures.

4 Results and discussion

4.1 Structural analysis

To scrutinize the crystallite size and phase structure, XRD pattern of PVP capped CdS nanostructures synthesized at different temperatures is depicted in Fig. 2. XRD pattern is recorded from a diffraction angle of 20° to 80° and compared with JCPDS card No. 892944. The comparative pattern validates the formation of hexagonal wurtzite structure.

This pattern exhibits various sharp and intense peaks signifying the polycrystalline nature of CdS nanostructures. With the increasing synthesizing temperature, intensity of various planes increased but no shifting in peak position is observed. Increasing intensity of various peaks showed better crystallinity that leads to decreasing value of strain and dislocation density with the temperature that clearly visible in Table 1. Growth of some planes gets increased at the cost of other reflections with increasing energy in terms of temperature that is clear in the XRD pattern.

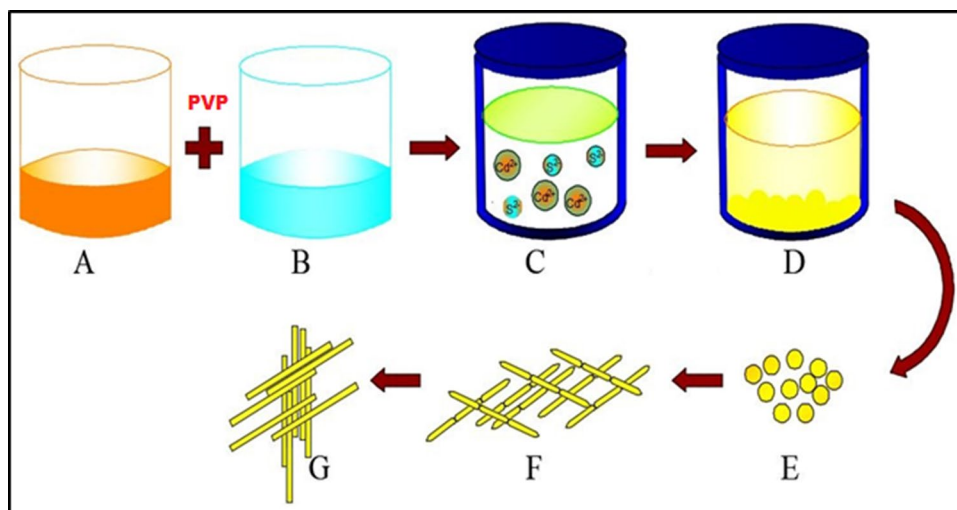
The structural parameter viz. average crystallite size and micro strain are extracted from XRD data. Debye Scherer formula is used to estimate the average crystallite size of CdS nanostructures [18] as shown in Eq. (1):

$$D = k\lambda/\beta\cos\theta \quad (1)$$

where k represents crystal shape constant having value 0.94, λ is the wavelength of X-ray, β is full-width half maxima and θ represents Bragg's diffraction angle.

The micro strain is evaluated by using Eq. (2):

Fig. 1 Schematic diagram of synthesis of PVP capped CdS nanostructures. **a** 0.12 M cadmium acetate dihydrate precursor solution. **b** 0.34 M thiourea precursor solution. **c** Teflon lined autoclave containing mixture of two precursor solution. **d** CdS precipitation after solvothermal growth. **e** CdS nuclei. **f** Oriented alignment of CdS nanostructures. **g** Final growth of CdS nanostructures



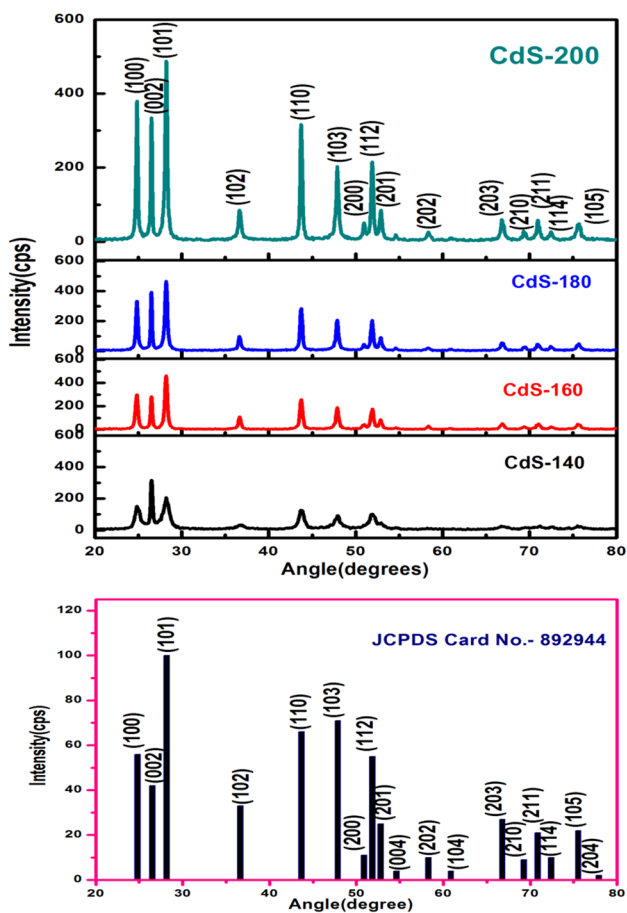


Fig. 2 XRD pattern of PVP capped cadmium sulfide nanostructures at different temperatures and compared with standard JCPDS Card

$$\epsilon = \beta / 4 \tan \theta \tag{2}$$

The dislocation density is also calculated by using the following equation [19]:

$$\delta = 1/D^2 \tag{3}$$

As the synthesis temperature increases, crystallite size increased from 19.22 to 36.55 nm and correspondingly, the value of micro strain decreased from 7.56×10^{-3} to 3.58×10^{-3} (Fig. 3). The micro strain is common in nanostructures and comes from dislocations, vacancies, grain boundaries and shear planes. The decreasing trend in the value of dislocation density, as CdS synthesized at a series

of different temperature from 140 °C to 200 °C, lead to better crystallinity. The Lattice constants for hexagonal system are calculated from Bragg’s formula [20] as tabulated in Table 2. The lattice parameters show quite good concurrence with the standard values ($a=4.14, c=6.722$) of JCPDS card No. 892944. Generally, lattice constant is average value of physical dimensions of unit cells in a crystal lattice. The value of lattice constant in nano crystals slightly deviates from its original value due to strains or defects introduced during synthesis and surface reconstruction that is clearly indicated in the values of lattice constant.

Large distributions of crystallographic orientations are present in polycrystalline sample that can be fully random or the preferred one. To evaluate the texture coefficient and to explore the preferred orientation for CdS nanostructures following equation [18] is used.

$$\text{Texture coefficient} = \frac{I(hkl)}{I_0(hkl)} \left\{ \frac{1}{n} \sum \frac{I(hkl)}{I_0(hkl)} \right\}^{-1} \tag{4}$$

where $I(hkl)$ represents the relative measured intensity of planes of CdS nanostructures and $I_0(hkl)$ represents the relative intensity of corresponding planes in JCPDS data. The maximum value of texture coefficient is n and n is number of peaks. The value of texture coefficient indicates the preferred orientation of nanostructures along the corresponding miller plane. The values of texture coefficients are shown in Table 3.

A value greater than 1 indicates the preferred orientation for that plane. It is evident from Table 3 that the plane (103) is not preferred directions at any temperature. The texture coefficient of plane (100), (101) and (110) are increased and for plane (002), it is decreased with temperature as shown in Table 3. It is concluded that more and more planes orient in the direction of (100), (101) and (110) plane with increase in temperature. It may also be concluded that crystallographic orientations get reoriented at the expense of other orientation with temperature.

4.2 Morphological studies

The morphology of synthesized CdS nanostructures at different temperature, keeping all the parameters constant, is examined with the FESEM. Figure 4a–d shows the micrographs of CdS synthesized at temperature 140 °C, 160 °C, 180 °C and 200 °C, respectively.

Table 1 Average crystallite size, lattice strain and dislocation density of PVP capped CdS nanostructures

	CdS-140	CdS-160	CdS-180	CdS-200
Crystallite size	19.22 nm	29.49 nm	33.75 nm	36.55 nm
Lattice strain	7.56×10^{-3}	4.58×10^{-3}	3.96×10^{-3}	3.58×10^{-3}
Dislocation density	$2.71 \times 10^{15} \text{ m}^{-2}$	$1.15 \times 10^{15} \text{ m}^{-2}$	$0.88 \times 10^{15} \text{ m}^{-2}$	$0.75 \times 10^{15} \text{ m}^{-2}$

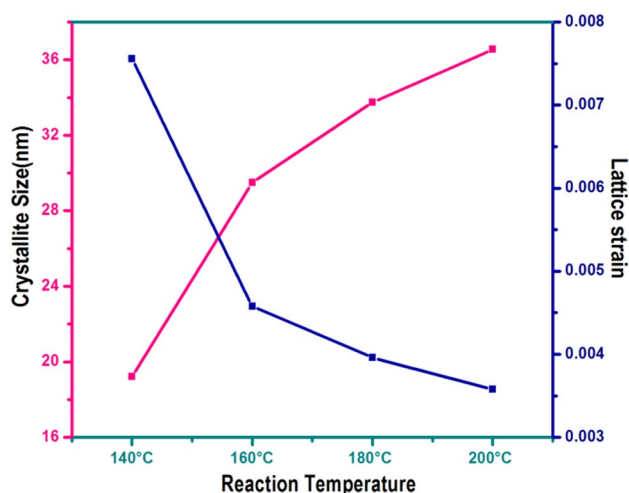


Fig. 3 Average crystallite size and strain in nanostructures with respect to synthesizing temperature

Table 2 Structural parameter of PVP capped CdS nanostructures

Sample	Crystal structure	Lattice parameter (Å)	Preferred growth direction
CdS-140	Hexagonal	$a=4.137, c=6.710$	(002)
CdS-160	Hexagonal	$a=4.138, c=6.720$	(101)
CdS-180	Hexagonal	$a=4.134, c=6.719$	(101)
CdS-200	Hexagonal	$a=4.137, c=6.722$	(101)

Table 3 Texture coefficient analysis

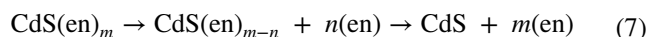
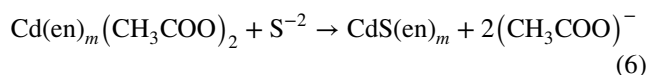
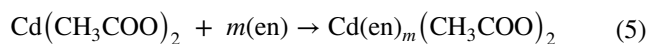
	CdS-140	CdS-160	CdS-180	CdS-200
(100)	1.26	1.49	1.60	1.76
(002)	3.38	2.54	2.18	2.06
(101)	0.96	1.19	1.25	1.30
(110)	0.72	1.09	1.15	1.24
(103)	0.61	0.75	0.77	0.79

Nanorods mesh can be easily seen for all the CdS samples. These micrographs clearly showed that nanorods are grown with high density. FESEM images demonstrate that CdS synthesized at 140 °C are in initial growth stage of nanorods after nucleation. While the CdS nanorods synthesized at 160 °C exhibited high yield and better uniformity and length of nanorods also get increased. Figure 4c and d presented that CdS nanorods synthesized at 180 °C and 200 °C are broken and fragmented into small parts at higher temperatures.

Figure 4e demonstrates the EDS spectra of CdS nanorods obtained at 160 °C. The EDS spectrum reveals the presence of Cd and S, without any impurity peaks, signifying the pure

phase of CdS nanorods. The average atomic percentage of Cd and S is found to be 50.92 and 49.08, respectively that corresponds to almost 1:1 stoichiometry of CdS nanorods.

Solvent plays a very crucial role on the surface morphology in solvothermal synthesis. Furthermore, mixing of solvent in the synthesis of nanostructures is also very popular. Polyamines such as ethylenediamine (en) conventionally used as shape modifying agent and stabilizer in growth of chalcogenide nanostructures. Ethylenediamine ($C_2H_4(NH_2)_2$) is strong basic amine that can act as chelating ligand for cadmium ions and form Cd–en complex. However, if only water is used as solvent, then no complex is formed. Cadmium and sulfur source get hydrolysed in water and produce Cd^{+2} and S^{-2} resulting into the formation of CdS. This Cd–en complex form a network which leads the ultimate morphology of CdS. Cd–en complex interact with suitable sulfur source during solvothermal treatment and sulfurization take place. At higher temperature, the extra amount of adsorbed en on surface of CdS gets degraded. The rate of CdS generation can be influenced by solvent ratio leading to different morphologies of synthesized CdS nanostructures [21, 22]. From above aspects, a general reaction mechanism is predicted here.



In our case, cadmium acetate reacts with en and form complex. Thiourea decomposes into S^{-2} ions in basic medium and reacts with Cd–en complex. Finally, pure CdS is formed at higher temperature during solvothermal synthesis.

4.3 FTIR studies

Fourier Transform Infrared Spectroscopy is used to study the infrared spectrum of absorption or emission of sample. FTIR is utilized to examine the composition and quality of PVP capped CdS nanostructures prepared with ethylenediamine as solvent. Figure 5 shows the FTIR spectrum of cadmium sulfide nanostructures synthesized at 160 °C by solvothermal route.

The broad absorption peak ranges from 3200 to 3650 cm^{-1} corresponds to O–H stretching of H_2O that specifies the water absorption on the surface. The strong absorption band at 1654 cm^{-1} is attributed to C=O stretching of acetone that generally ranges from 1650 to 1720 cm^{-1} . The small and weak absorption peak near 405 cm^{-1} corresponds to characteristic peak of CdS [23, 24].

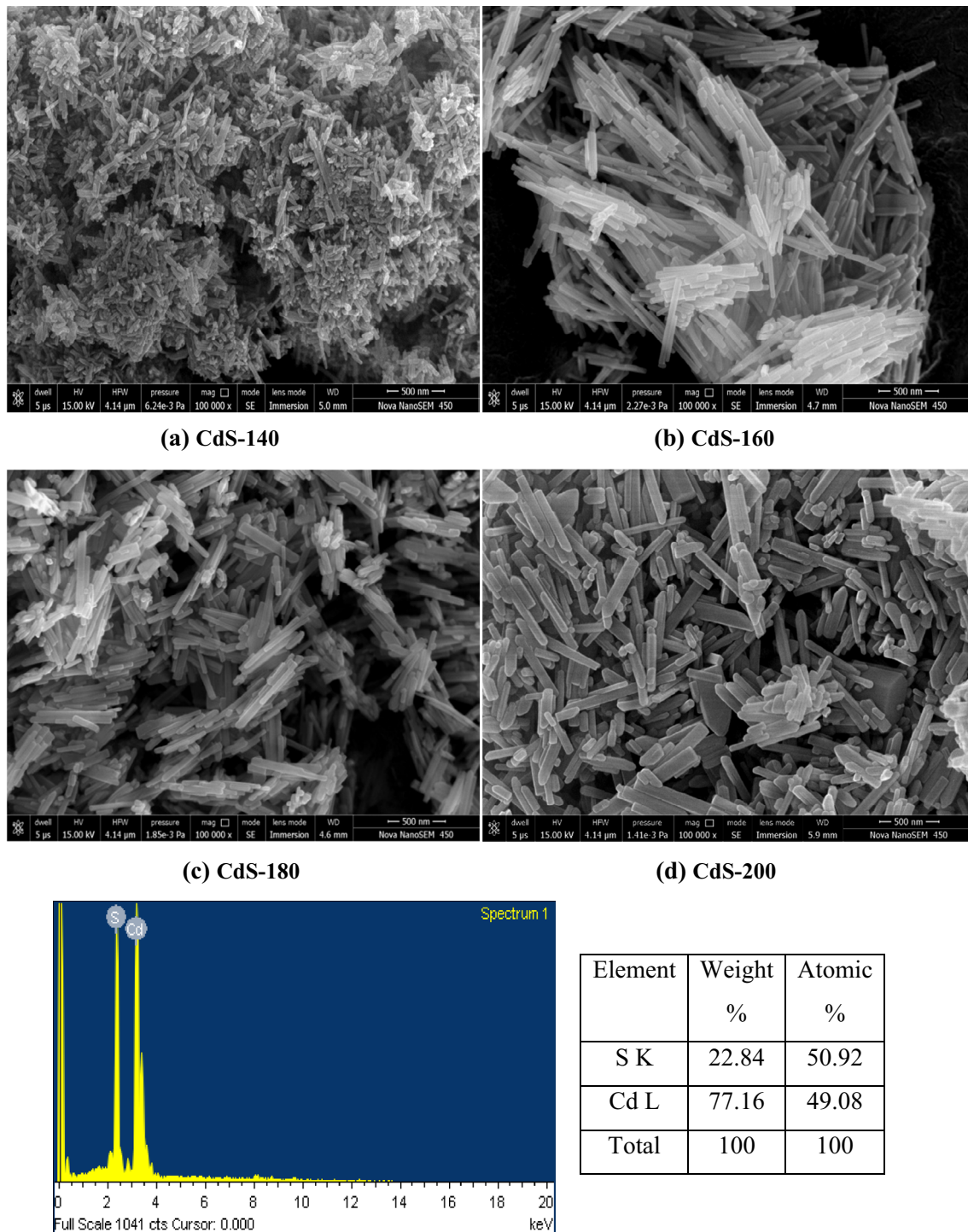


Fig. 4 FESEM images of PVP capped CdS nanostructures synthesized at: **a** 140 °C, **b** 160 °C, **c** 180 °C and **d** 200 °C and **e** EDS spectra of PVP capped CdS nanostructures

Two bands centered at 1040 and 1373 cm^{-1} are ascribed to C–N stretching vibrations of aromatic amines [25]. The small and weak absorption band near 600 cm^{-1} corresponds to S–O bonding. PVP controlled CdS nanostructures show a broad absorption peak from 1250 to 1600 cm^{-1} that

corresponds to C–N and C=O stretching vibrations of PVP. The small peaks observed at 1447 and 2936 cm^{-1} correspond to C–H stretching due to presence of PVP [26, 27]. This indicates the surface of CdS nanostructures are reconstructed by PVP.

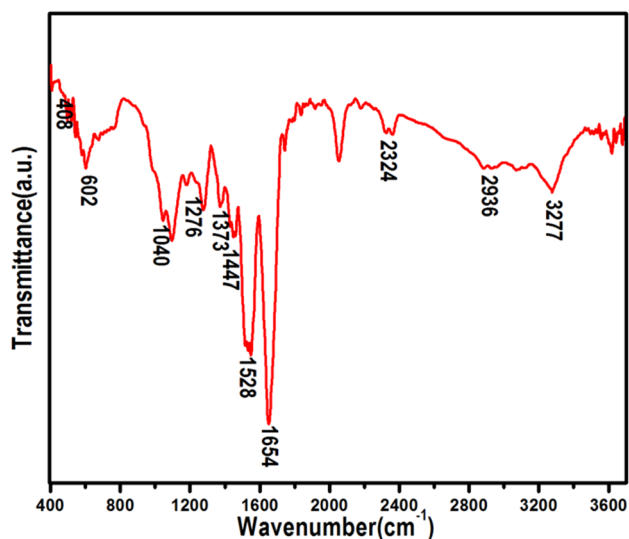


Fig. 5 FTIR Spectra of PVP capped CdS nanostructures

4.4 Optical properties

4.4.1 UV–Vis spectra

Morphology of nanostructures strongly affects the optical properties of cadmium sulfide. So, the UV–Vis optical absorption spectra of as-synthesized CdS nanostructures are recorded using a UV–Vis spectrophotometer (Fig. 6).

All these cadmium sulfide samples synthesized at different temperatures show sharp absorption spectra in the wavelength range of 300–800 nm. The absorption edge is observed at 449 nm, 455 nm, 467 nm and 471 nm for CdS nanostructures at 140 °C, 160 °C, 180 °C and 200 °C, respectively. The absorption edges are observed at wavelength smaller than bulk, which is about 515 nm, indicated the slight blue shift in absorption edge.

The optical band gap of CdS with different morphology is estimated by Tauc's formula from absorption data according to this equation [28]:

$$\alpha = \frac{A(h\nu - E_g)^n}{h\nu} \quad (8)$$

where α is absorption coefficient, $h\nu$ is photon energy, A is constant, E_g is band gap energy and n is equal to 1/2 or 2 for direct or indirect band gap, respectively. Figure 7 shows the corresponding optical band gap of CdS nanostructures by plotting a graph between $(\alpha h\nu)^2$ and $h\nu$ according to Tauc's equation.

The value of energy band gap of CdS nanostructures are calculated to be 2.76 eV, 2.72 eV, 2.65 eV and 2.62 eV synthesized at 140 °C, 160 °C, 180 °C and 200 °C, respectively. The absorption edge get shifted to higher

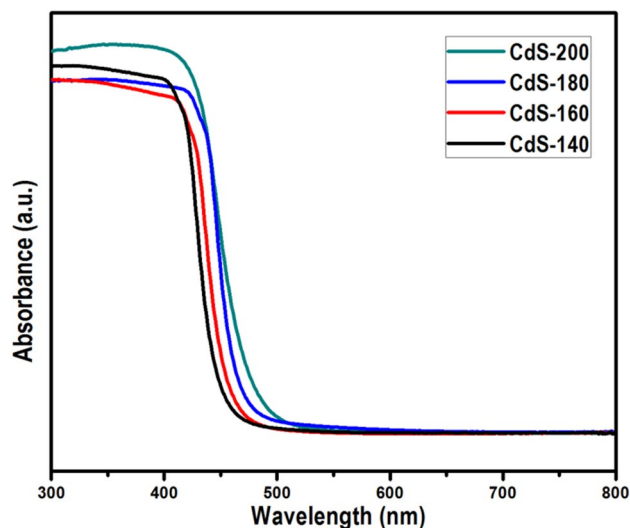


Fig. 6 UV–Vis Spectra of PVP capped CdS nanostructures

wavelength side, as solvothermal temperature increases, indicates the decrease in band gap. The decrease in value of band gap for CdS samples with temperature are in good agreement with the crystallite size and crystallinity of samples as extracted from XRD. The increased value of band gap of CdS nanostructures as compared to bulk CdS ($E_g = 2.42$ eV) indicates the weak quantum confinement associated with nanostructures [29].

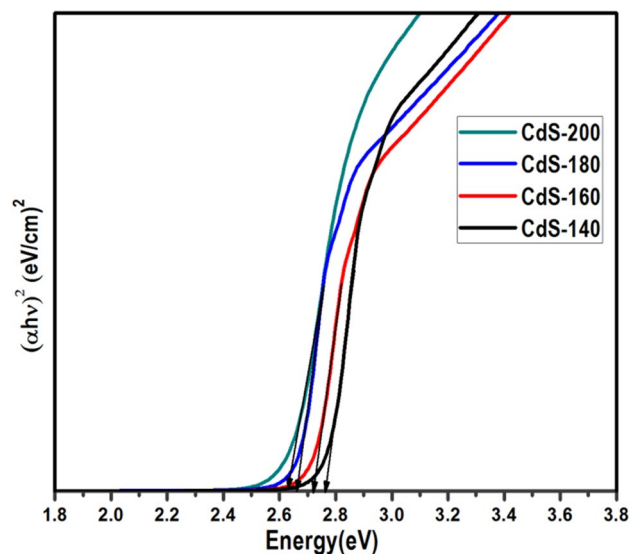


Fig. 7 Tauc plot of CdS nanostructures synthesized solvothermally at different temperatures

4.4.2 Photoluminescence spectra

A room temperature photoluminescence (PL) spectrum is sensitive and advantageous tool to explore the optical and electronic properties of semiconducting nanostructures. PL spectra involves the band edge transitions or defect transition. It is a major technique to examine the recombination efficiency of photo generated electron–hole pairs. Light is made to fall on the sample and electrons of molecule absorb energy to move into permissible excited states. After absorbing the photons, molecules undergo some internal energy distribution (non-radiation losses) resulted into emission of smaller energy photons. Photoluminescence spectrum for all the samples, i.e., CdS synthesized at 140 °C, 160 °C, 180 °C and 200 °C, are recorded and are shown in Fig. 8.

In the present study, samples are excited by Xenon light of 460 nm wavelength, a low intensity broad emission peak is observed for all the CdS samples. It can be seen that a very stable emission peak around at 529 nm is observed in all the cases. A slight blue shift is observed in the CdS sample synthesized at 140 °C. The observed slight shift in the peak position of emission spectrum can be assigned to size effect in nanostructures. The band position at 529 nm corresponds to green emission that is associated with the emission due to electronic transition from conduction band to acceptor level. The origin of acceptor level is attributed to sulfur interstitials which is supported by other previous experimental demonstrations [30]. In case of semiconducting nanostructures, defect levels or deep trap sites are created within the band gap of material. This will cause the broadening of PL spectra as well as deviation from defect free ideal energy band gap value of semiconductor. As-synthesized CdS nanostructures

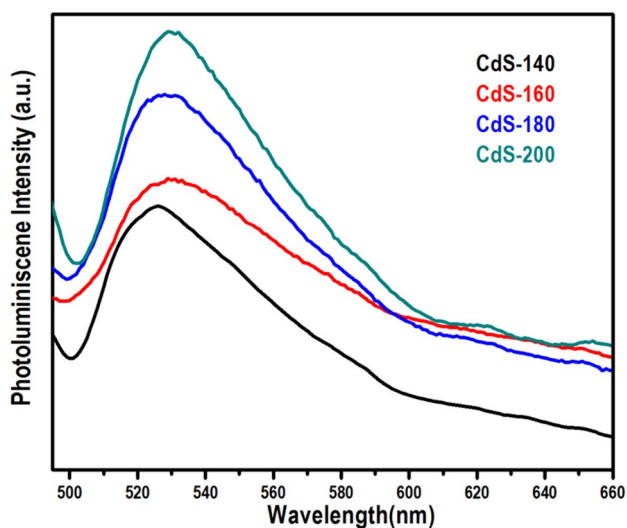


Fig. 8 Photoluminescence Spectra of PVP capped CdS nanostructures

are polycrystalline so composed of large number of grains and grain boundaries may have obstructed the significant emission. This study also concluded that polycrystalline cadmium sulfide with small defects might be beneficial for photo catalytic activity, sensing and for particular optoelectronic devices.

4.5 Electrical properties

Room temperature current voltage characteristic (IVC) is measured for cadmium sulfide nanostructures. Cylindrical pellets of 10 mm diameter of synthesized CdS nanoparticles are made by applying a pressure of 4–5 tones/cm² by hydraulic press. Pellets are sintered at 300 °C for 20 min in furnace having temperature and time controlled system. Both the sides of pellets are coated with silver paste for electrical measurement. *I–V* measurements are carried out for all as CdS pellets sample by using two probe setup supported with Keithley 2400 series source meter in voltage range from (– 10 to 10) volt as shown in Fig. 9.

A non-linear behavior of *I–V* characteristics is observed. This non-linear behavior may be due to formation of Schottky contacts between silver and CdS nanostructures [31]. Schottky barrier is generally a potential energy barrier formed at metal–semiconductor junction when work function of metal is higher than the work function of semiconductor material. This will result into formation of Schottky barrier having valuable high speed rectifying properties. It is clearly evident from *I–V* characteristics that value of current get increased across the voltage of – 10 to 10 V with increase in temperature. Grain boundaries play a very crucial role in electrical transport

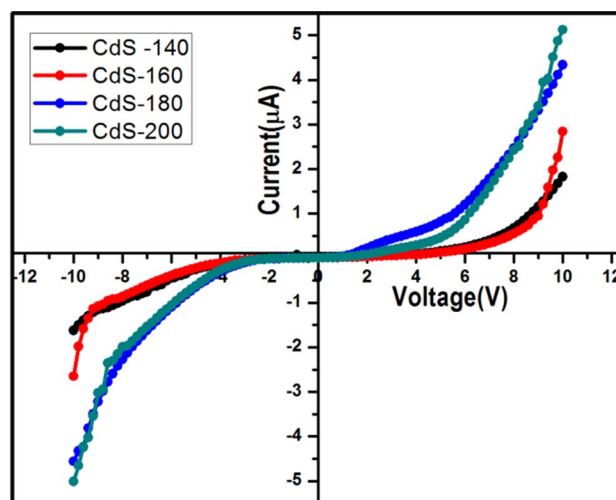


Fig. 9 *I–V* Characteristics of CdS nanostructures synthesized at different temperatures

properties of polycrystalline material. Grain boundaries play the role of potential barrier and scattering of charge carriers with these grain boundaries. An increment in crystallite size reduces the number of grain boundaries leading to refinement in crystallinity as discussed in XRD analysis. Hence, charge carriers undergo lesser number of scattering with increase in temperature and resulted into increment in current values. With temperature, an increment in value of conductivity might be expected. Optical band gap of CdS nanostructures is found to be decreased with increase in temperature, hence, electrical current get increased with temperature. We observed the maximum electrical current for cadmium sulfide nanostructures synthesized at 200°C due to large crystallite size [32, 33]. Previous studies suggest that schottky barrier manifests both low forward voltage drop and high reverse bias current and extensively utilized in large number of electronic devices in electronic industry for high frequency application [34].

5 Conclusions

The II–VI binary semiconducting CdS nanostructures are synthesized solvothermally by controlling the reaction time and precursor concentration. The role of different temperature on the different properties of CdS nanorods is investigated. From this study, we conclude that structural study confirmed the hexagonal wurtzite structures of CdS nanostructures. Nanorods like morphology are confirmed by FESEM analysis. The quantitative EDS analysis exhibited almost 1:1 stoichiometric ratio for CdS nanostructures. FTIR spectroscopy confirmed the composition of PVP capped CdS nanoparticles with ethylenediamine as solvent. The UV–Vis spectroscopy revealed that optical band gap increased at low solvothermal temperature indicating confinement effects in CdS nanostructures. While photoluminescence spectra corresponds to green emission which is associated to electronic transition from conduction band to acceptor level generated due to interstitial sulfur. Current voltage characteristics demonstrate that a schottky contact is formed between silver and CdS nanoparticles which is utilized in huge variety of high frequency applications in electronics. This analysis suggests utilization of CdS nanostructures for gas sensing, optoelectronic applications and for excellent photo catalytic activities in terms of solar-fuel generation and environmental purification.

Acknowledgement The authors acknowledge Director, NIT Kurukshetra, India for providing XRD, UV, PL and FTIR characterization

facilities. They also acknowledge IUAC, New Delhi, India for providing financial support in form of project (project no.-IUAC/XIII.7/UFR-63305). Authors express thanks to Material Research Centre, Malaviya National Institute of Technology, Jaipur for providing FESEM characterization facility.

References

1. K.V. Shanavas, S.M. Sharma, I. Dasgupta, A. Nag, A. Hazarika, D.D. Sarma, *J. Phys. Chem. C* **116**(11), 6507–6511 (2012)
2. J.M. Kephart, R.M. Geisthardt, W.S. Sampath, *Prog. Photovolt.* **23**(11), 1484–1492 (2015)
3. R. Ochoa-Landín, J. Sastre-Hernández, O. Vigil-Galan, R. Ramirez-Bon, *Sol. Energy* **84**(2), 208–214 (2010)
4. L. Cheng, Q. Xiang, Y. Liao, H. Zhang, *Energy Environ. Sci.* **11**(6), 1362–1391 (2018)
5. Q. Xiang, F. Cheng, D. Lang, *ChemSusChem* **9**(9), 996–1002 (2016)
6. S.A. Vanalakar, V.L. Patil, P.S. Patil, J.H. Kim, *New J Chem.* **42**(6), 4232–4239 (2018)
7. K. Deng, L. Li, *Adv Mater.* **26**(17), 2619–2635 (2014)
8. X.X. Yu, H. Yin, H.X. Li, W. Zhang, H. Zhao, C. Li, M.Q. Zhu, *Nano Energy* **34**, 155–163 (2017)
9. M.A. Kamran, R. Liu, L.J. Shi, B. Zou, Q. Zhang, *J. Phys. Chem. C* **117**(34), 17777–17785 (2013)
10. A. Bathla, C. Narula, R.P. Chauhan, *J. Mater. Sci.: Mater. Electron.* **29**(8), 6225–6231 (2018)
11. W. Gong, Z. Zheng, J. Zheng, X. Hu, W. Gao, *J. Appl. Phys.* **102**(6), 064304 (2007)
12. K. M. Chintala, S. Panchal, P. Rana, R. P. Chauhan, *J. Mater. Sci.: Mater. Electron.* **27**(8), 8087–8093 (2016)
13. K.M. Koczur, S. Mourdikoudis, L. Polavarapu, S.E. Skrabalak, *Dalton Trans.* **44**(41), 17883–17905 (2015)
14. N. Zhao, J. Peng, G. Liu, Y. Zhang, W. Lei, Z. Yin, L. Jiuqiang, M. Zhai, *J. Mater. Chem. A* **6**(38), 18458–18468 (2018)
15. W. Qingqing, Z. Gaoling, H. Gaorong, *Materials* **59**(21), 2625–2629 (2005)
16. H. Qi, J.F. Huang, L.Y. Cao, J.P. Wu, D.Q. Wang, *Ceram. Int.* **38**(3), 2195–2200 (2012)
17. Q. Xia, X. Chen, K. Zhao, J. Liu, *Mater. Chem. Phys.* **111**(1), 98–105 (2008)
18. B.D. Cullity, S.R. Stock, *Elements of X-Ray Diffraction*, 3rd edn. (Prentice-Hall, New Jersey, 2001), pp. 167–171
19. G.K. Williamson, W.H. Hall, *Acta Metall.* **1**(1), 22–31 (1953)
20. M.A. Abdulsattar, *Solid State Sci.* **13**(5), 843–849 (2011)
21. Y. Li, Y. Hu, S. Peng, G. Lu, S. Li, *J. Phys. Chem. C* **113**(21), 9352–9358 (2009)
22. A. Phuruangrat, T. Thongtem, P. Pongphab, S. Thongtem, *Solid State Sci.* **14**(8), 1023–1029 (2012)
23. N. Qutub, B.M. Pirzada, K. Umar, S. Sabir, *J. Environ. Chem. Eng.* **4**(1), 808–817 (2016)
24. H. Wang, P. Fang, Z. Chen, S. Wang, *Appl. Surf. Sci.* **253**(20), 8495–8499 (2007)
25. P. Dalvand, M.R. Mohammadi, D.J. Fray, *Mater. Lett.* **65**(9), 1291–1294 (2011)
26. Y. Wu, L. Wang, M. Xiao, X. Huang, *J. Non-Cryst. Solids* **354**(26), 2993–3000 (2008)
27. L. Saravanan, S. Diwakar, A. Pandurangan, R. Jayavel, *Nanomater. Nanotechnol.* **1**(2), 42–48 (2011)
28. V. Kumar, S. Kumar, S. Kumar, S. K. Chakarvarti, *J. Mater. Sci.: Mater. Electron.* **22**(4), 335–338 (2011)

29. W. Xu, Y. Wang, R. Xu, S. Liang, G. Zhang, D. Yin, J. Mater. Sci. **42**(16), 6942–6945 (2007)
30. O. Vigil, I. Riech, M. Garcia-Rocha, O. Zelaya-Angel, J. Vac. Sci. Technol. A **15**(4), 2282–2286 (1997)
31. M. Sharma, S. Kumar, L.M. Sharma, T.P. Sharma, M. Husain, Physica B **348**(1–4), 15–20 (2004)
32. A.A.M. Farag, I.S. Yahia, M. Fadel, Int. J. Hydrogen Energy. **34**(11), 4906–4913 (2009)
33. S. Chander, A. Purohit, C. Lal, M.S. Dhaka, Mater. Chem. Phys. **185**, 202–209 (2017)
34. B.L. Sharma, *Metal-Semiconductor Schottky Barrier Junctions and Their Applications* (Springer, New York, 2013)

Publisher's Note Springer Nature remains neutral with regard to jurisdictional claims in published maps and institutional affiliations.